THE ASTROPHYSICAL JOURNAL, 427:125–133, 1994 May 20

ORIENTATION MODELING OF RADIO GALAXY AND QUASAR PROPERTIES: EVIDENCE FOR A UNIFIED MODEL

MATTHEW L. LISTER,[1,2] J. B. HUTCHINGS,[3] AND ANN C. GOWER[1]
Received 1993 September 7; accepted 1993 November 15

ABSTRACT

We discuss the statistics of projection on the sky of a simple model for radio sources. The model has a core and two hot spots at unequal distance with an overall structure which is bent at the core. We examine the distributions of the observed sizes and bend angles in 114 quasars and 78 radio galaxies with $z < 2$, from our own data. We find that the observations are well matched by this model with (*a*) a size distribution matching the observed one, (*b*) core-hotspot length differences between 0 and 45 kpc, and (*c*) bend angles distributed between 0° and ~25°, where quasars are seen within 50° of the source axis, and radio galaxies are seen at greater angles. We discuss the implications of these fits to unified models and source evolution.

Subject headings: galaxies: active — methods: statistical — quasars: general — radio continuum: galaxies

1. INTRODUCTION: ORIENTATION EFFECTS

Knowledge of the orientation of an extragalactic radio source (EGRS) to our line of sight is an essential part of understanding its intrinsic structure and also of understanding possible strong selection effects. The most extreme case of the effects of orientation on observation is that of relativistic beaming. At radio wavelengths, a large fraction of the core luminosity from radio galaxies and quasars is thought to originate in relativistic bulk flows which, depending on orientation, may be Doppler-boosted toward the observer, thereby greatly enhancing the measured flux. This in turn may strongly affect the discovery of such sources and bias our statistics. A knowledge of the viewing angle is essential in understanding the true nature of such sources.

In all cases where there is direct observational evidence, radiation from active nuclei is seen to be nonisotropic, if not beamed. Thus such considerations are of importance generally. Unified schemes have been proposed (e.g., Barthel 1989; Padovani & Urry 1992; Scheuer 1987) which attempt to account for the differences between quasars and radio galaxies simply by orientation to the line of sight. While it is clear that orientation is important in many EGRSs, it is equally clear that intrinsic differences must exist between sources as they evolve individually and in cosmic time as a population. Thus, the interpretation of EGRSs is a complex exercise.

Since EGRSs have been found to have a wide variety of sizes and shapes, it is not possible to use simple deprojection methods such as those used to estimate the inclination angles of spiral galaxies. Several authors (Kapahi & Saikia 1982; Fokker 1986; Hough & Readhead 1989) have discussed methods of using the observed characteristics of EGRSs as orientation indicators. The most popular and easily measured quantities to use are sizes, bends, and core–hot spot distance ratios, as they are all subject to distortion by projection on the sky. Another popular orientation indicator is the ratio of core to extended flux, or *core fraction*. According to the relativistic beaming model, a source aligned close to the line of sight would have its core flux greatly amplified due to Doppler boosting, while the radiation from the extended structure, being less collimated and originating in less relativistic regions, would not be as greatly affected. The core fraction could in theory be used as an indicator of source orientation. However, in Lister, Gower, & Hutchings (1994 [LGH]), we present evidence showing that the core fraction is too strongly influenced by individual source evolution to be used as an orientation indicator, so we choose not to employ it in this paper. We will instead investigate the three morphological properties mentioned above for our large NRAO–VLA[4] quasar sample (Gower & Hutchings 1984 [GH]; Hutchings, Price, & Gower 1988 [HPG]; Neff, Hutchings, & Gower 1989 [NHG]; Neff & Hutchings 1990 [NH]; LGH) and attempt to fit them with a simple class of orientation-biased models. We also look for consistency with recent radio galaxy data presented in Hutchings et al. (1994).

In Figure 1, we illustrate a typical double-lobed EGRS. The notable features of the source are the unresolved core component, identified with the active nucleus, and two large radio lobes located on opposite sides of the core. Each lobe contains a hot spot, which generally lies at its outermost edge, and is considered to arise where the end of the radio jet encounters the intergalactic medium. The core and hot spots of EGRSs are generally noncollinear due to misalignment or bending of the radio jets. The possible origins of these bends will be the topic of further discussion in § 4.3.

If the EGRS in Figure 1 is viewed near to end-on, there are several significant projection effects. First, the apparent distance between the hot spots is reduced. Second, the apparent bend angle is generally increased, although it may be reduced if the intrinsic bend is large. Finally, for an intrinsically bent source, one lobe will suffer more foreshortening than the other, changing the ratio of the observed core–hot spot distances. For our sample we measured the latter ratio (hereafter Q) following Teerikorpi's (1984) definition as the ratio of L_1 to L_2 that is less than or equal to unity. We measured bend angles and sizes according to Figure 1, with the latter quantity being defined as

[1] Department of Physics and Astronomy, University of Victoria, P.O. Box 3055, Victoria, Canada, BC V8W 2Y2.
[2] Present Address: Department of Astronomy, Boston University, 725 Commonwealth Avenue, Boston, MA 02215.
[3] Dominion Astrophysical Observatory, National Research Council of Canada, 5071 West Saanich Road, Victoria, Canada, BC V8X 4M6.

[4] The National Radio Astronomy Observatory is operated by Associated Universities, Inc., under cooperative agreement with the National Science Foundation.

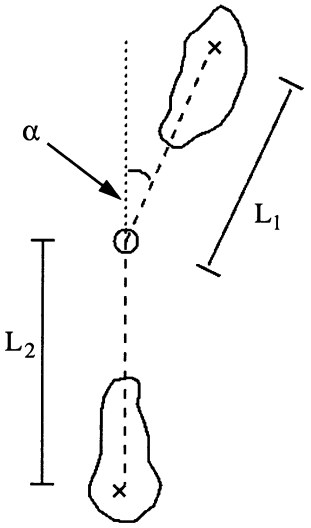

FIG. 1.—A canonical extragalactic radio soure (EGRS), defining the model parameters. On either side of an unresolved core component are two radio lobes, each containing a hot spot (×) located at a distance L from the core. The intrinsic bend of the source is described by the bend angle (α). The largest apparent size (LAS) is defined as the linear distance between the two hot spots, and the core–hot spot distance ratio (Q) is taken to be the ratio of L_1 to L_2 that is always less than unity.

the linear distance between the hot spots. Since all these measured quantities are related to orientation, we wish to use their correlations and distributions in a real database to fit some simple orientation-biased models.

2. OBSERVATIONAL DATA

We use the quasars from our earlier papers as they were selected and measured in a uniform way. The ~250 objects were chosen on the basis of redshift and total 2.7 GHz power only, with no bias by spectral index or morphology. From these, we have assembled a subset consisting only of double-lobed quasars with a detected core component. The latter criterion was necessary to minimize the errors in measuring bend angles and core–hot spot distances that arise from using poorly defined optical core positions. Table 1 summarizes the measures in this database. We also use the same measures in the radio galaxy samples described by Hutchings et al. (1994). In that paper considerable effort was put into obtaining good optical positions for the cores, since many radio galaxies have no detected cores.

While our papers describe the sample selections in detail, we note here that in all our samples, selection was made without reference to source morphology or spectral index. The samples were chosen from a wide variety of catalogs with the object of sampling the 2.7 GHz luminosity/redshift plane as widely as possible. In the case of the radio galaxy sample, we attempted also to match the quasar sample distribution in this plane. Whatever selection effects that are present are mixed, and as far as we can see, not critical in the double-lobe sources that are used in the present discussion.

There are claims in the literature that EGRS properties evolve strongly with redshift (e.g., Barthel & Miley 1988). As discussed in NH (and also by Chyzy & Zieba 1993; Gopal-Krishna & Kulkarni 1992) we have found that the largest linear sizes of quasars decrease with increasing redshift. We find no strong trend in either the bend angle or Q-value distributions for the triple sources in our sample up to $z = 2$. A Kolmogorov-Smirnov (K-S) test on the bend angle distributions for quasars with $z < 1$ and $1 < z < 2$ shows that they are the same at the 99.6% confidence level. The Q distributions are similar at 93% confidence (although NH discuss a possible trend of this distribution with redshift). These findings are consistent with those of Kapahi (1990), who looked at the Q and bend angle values for the triple radio quasars in the 3CR sample and found no trends with redshift. There does appear to be some evolution in these parameters past $z = 2$, however, although numbers are very small, so to avoid complications involving evolutionary effects, we have included only quasars with $z < 2$, leaving a total of 114 triple sources in our subsample.

The quasar data and the appropriate references are presented in Table 1. Columns (1) and (2) give the IAU source name and redshift taken from the Hewitt & Burbidge (1989) catalog. Column (4) lists the largest apparent size (LAS) in arcseconds as measured from the radio maps. Its value converted to kiloparsecs is given in column (5). As in our other papers, we have adopted a flat spacetime cosmological model where $H_0 = 100$ km s^{-1} Mpc^{-1} and $q_0 = 0.5$ in converting the angular sizes to distances. Columns (3) and (6) give the core–hot spot distance ratio (Q) and bend angle, respectively. In our original papers, every attempt was made to ensure that the measurements were made in a consistent manner, but in practice, the measurement of bend angles is complicated by the effects of resolution and sensitivity on the maps. In a few cases, it was difficult to determine the exact location of the hot spots, which introduced errors in the measured Q-values. However, we regard the Q-values as good to 10% for almost all the sources.

3. SAMPLE PROPERTIES

In Figure 2 we have plotted apparent size (in kpc) versus apparent bend angle for the sample. The well-defined upper envelope to the distribution is consistent with that seen by Kapahi & Saikia (1982) in their sample of 78 radio quasars. Hough & Readhead (1989) also found a similar trend in a

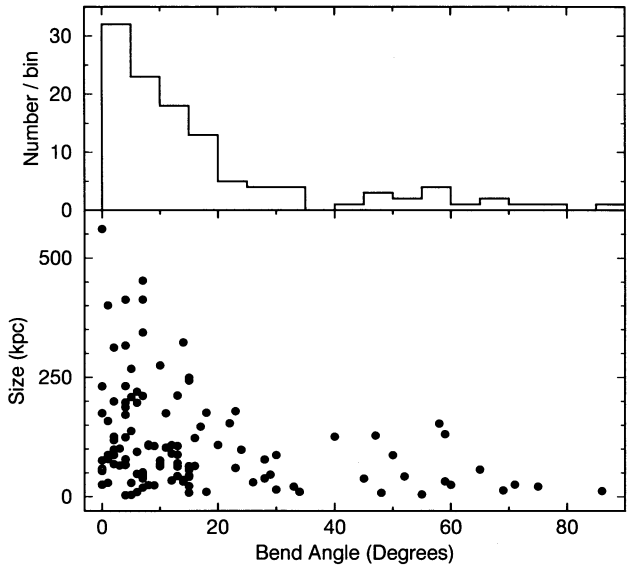

FIG. 2.—Largest apparent size vs. bend angle for the quasar sample. The lower panel shows a well-defined upper envelope consistent with projection effects.

TABLE 1

RADIO QUASAR DATA

Name (1)	z (2)	Q[a] (3)	LAS[b] (″) (4)	Size[c] (kpc) (5)	Bend (°) (6)	Ref. (7)
0003+158.....	0.450	0.89	31.5	107	8	HPG
0006+014.....	1.302	0.67	15	65	16	NHG
0007+332.....	0.743	0.86	77.2	313	2	HPG
0017+257.....	0.284	0.93	48.2	128	47	GH
0041+119.....	0.228	0.57	46	106	9	LHG
0044+030.....	0.624	0.47	11.6	45	7	HPG
0118+034.....	0.765	0.91	43	175	11	HPG
0119−046.....	1.948	0.80	3.6	15	30	NHG
0127+233.....	1.459	0.40	2.8	12	86	NHG
0133+207.....	0.425	0.82	70	232	4	HPG
0137+012.....	0.258	0.74	35	88	1	GH
0159−117.....	0.670	0.11	15.3	60	23	HPG
0222−008.....	0.687	0.88	16	63	13	HPG
0238+100.....	1.816	0.60	16	67	4	NHG
0300−004.....	0.693	0.77	8.0	32	14	HPG
0307+444.....	1.165	0.63	4.5	19	7	NHG
0340+048.....	0.357	0.88	34	103	11	HPG
0349−146.....	0.614	0.76	118	453	7	HPG
0352+123.....	1.616	0.60	9.0	38	45	NHG
0354+202.....	1.728	0.91	21	88	13	HPG
0409+229.....	1.215	0.93	5.0	22	75	NHG
0440−003.....	0.844	0.80	2.1	9	15	HPG
0446−208.....	1.896	0.89	51	211	7	NHG
0534−201.....	0.995	0.82	16.5	70	13	HPG
0553−205.....	1.544	0.96	5.0	21	33	NHG
0557−168.....	1.240	0.50	21	90	12	NHG
0704+384.....	0.579	1.00	21	79	1	HPG
0725+147.....	1.382	0.37	6.0	26	0	NHG
0736−019.....	1.033	0.53	9.0	38	28	NHG
0742+318.....	0.462	0.96	120	413	4	GH
0805+579.....	0.438	0.88	26	87	2	HPG
0810+327.....	0.842	0.48	26	108	12	HPG
0821+447.....	0.904	0.97	26	109	8	HPG
0827+193.....	0.658	0.79	24	94	6	HPG
0831+101.....	1.760	0.88	30	126	2	NHG
0846+100.....	0.366	0.72	69	212	13	GH
0856+124.....	1.760	0.41	30	126	40	NHG
0901+285.....	1.121	0.92	23	99	2	NHG
0903+169.....	0.411	1.00	54.1	176	18	HPG
0932+023.....	0.892	0.16	47	197	6	HPG
0937+391.....	0.618	0.86	52	200	2	HPG
0952+097.....	0.298	0.48	12.5	34	12	GH
1004+130.....	0.240	0.36	115	275	10	GH
1011−282.....	0.253	0.43	72.6	180	23	GH
1012+488.....	0.385	0.96	109	344	7	HPG
1015+277.....	0.469	0.89	22	76	0	HPG
1020−103.....	0.197	0.09	1.7	4	4	LHG
1022+194.....	0.828	0.59	14.2	59	0	HPG
1028+313.....	0.177	0.60	28	54	0	GH
1038+528.....	0.677	0.93	39	154	22	HPG
1104+167.....	0.634	0.98	48.5	188	4	HPG
1118+128.....	0.685	0.67	22	87	30	HPG
1130+106.....	0.540	1.00	3.7	14	69	HPG
1146+111.....	0.863	0.85	16.4	68	10	HPG
1156+631.....	0.594	0.75	58	220	6	HPG
1157+118.....	0.731	0.37	25	101	3	HPG
1217+023.....	0.240	0.95	135	323	14	GH
1222+216.....	0.435	0.85	17	57	65	HPG
1223+252.....	0.268	0.95	67	172	4	GH
1233+108.....	0.665	0.72	102	401	1	HPG
1243−072.....	0.267	0.41	9.8	25	0	GH
1253+104.....	0.824	0.92	23.8	99	24	HPG
1302−102.....	0.286	0.83	16	43	52	LHG
1335−061.....	0.625	0.79	11.3	44	13	HPG
1352−203.....	0.627	0.88	17	66	3	HPG
1400+162.....	0.244	0.83	36.1	87	50	GH
1415+172.....	0.821	0.52	6.2	26	71	HPG
1420+326.....	0.685	0.29	31	123	16	HPG
1423+242.....	0.649	0.76	20	78	28	HPG
1442+117.....	0.851	0.36	15.4	64	10	HPG
1458+718.....	0.905	0.83	2.5	11	34	HPG
1509+158.....	0.828	0.26	2.0	8	48	HPG
1522+155.....	0.361	0.63	25.8	79	4	HPG
1530+137.....	0.771	0.64	11.4	47	29	HPG
1540+110.....	0.992	0.93	37.4	159	1	HPG
1545+210.....	0.264	0.74	69	176	0	GH
1548+114.....	0.436	0.85	45.8	154	58	HPG
1606+180.....	0.346	0.75	12.9	38	7	HPG
1618+177.....	0.555	0.61	53.4	198	4	HPG
1623+173.....	0.552	0.80	32.1	119	2	HPG
1700+180.....	1.424	0.82	12	52	7	NHG
1704+608.....	0.371	0.79	67.5	209	5	HPG
1721+343.....	0.206	0.97	260	561	0	GH
1739+184.....	0.186	0.96	206	413	7	GH
1741+279.....	0.372	0.84	9.8	30	26	HPG
1807+279.....	1.760	0.55	8.5	36	14	NHG
1827+387.....	1.080	0.92	2.3	10	6	NHG
1830+285.....	0.594	0.98	28.6	109	20	HPG
1857+566[d].....	1.595	0.85	25	106	13	NHG
1924+507.....	1.098	0.60	16	69	2	NHG
2005−044.....	0.589	0.53	20.1	76	10	HPG
2025+117[d].....	1.920	0.93	56	231	0	NHG
2112+172.....	0.878	0.52	6.0	25	60	HPG
2131+175.....	1.215	0.78	32	138	5	NHG
2135−147.....	0.200	0.90	150	317	4	GH
2158+101.....	1.725	0.75	1.2	5	55	NHG
2201+315.....	0.298	0.83	91	249	15	GH
2209+080.....	0.484	0.56	11.9	42	15	HPG
2209+152.....	1.502	0.88	15	64	15	NHG
2217+08N.....	0.623	0.84	34	131	59	GH
2217+08S.....	0.228	0.92	116	268	5	GH
2223+210.....	1.959	0.22	5.5	23	15	NHG
2230+114.....	1.037	0.50	2.4	10	18	NHG
2249+185.....	1.757	0.83	1.0	4	5	NHG
2251+113.....	0.323	0.60	10.2	29	1	HPG
2251+134.....	0.549	0.55	6.6	24	9	HPG
2303−052.....	1.139	0.62	10.5	45	15	NHG
2305+187.....	0.313	0.59	20	56	15	GH
2314−116.....	0.549	0.65	39.8	147	17	HPG
2322+110.....	1.965	0.50	6.0	25	8	NHG
2325+269.....	0.875	0.61	7.0	29	5	HPG
2333+019.....	1.871	0.76	30	125	4	NHG
2349+327.....	0.659	0.55	62	243	15	HPG
2353+283.....	0.731	0.67	8.0	32	59	HPG
2354+144.....	1.810	0.92	11.5	48	6	NHG

[a] Core-hot spot distance ratio (see Fig. 1).

[b] Largest apparent size (see Fig. 1).

[c] Sizes in kpc were calculated assuming $H_0 = 100$ km s^{-1} Mpc^{-1} and $q_0 = 0.5$.

[d] These sources were remeasured using improved maps.

REFERENCES.—GH: Gower & Hutchings 1984; HPG: Hutchings, Price, & Gower 1988; LHG: Lister, Hutchings, & Gower 1994; NH: Neff & Hutchings 1990; NHG: Neff, Hutchings, & Gower 1989.

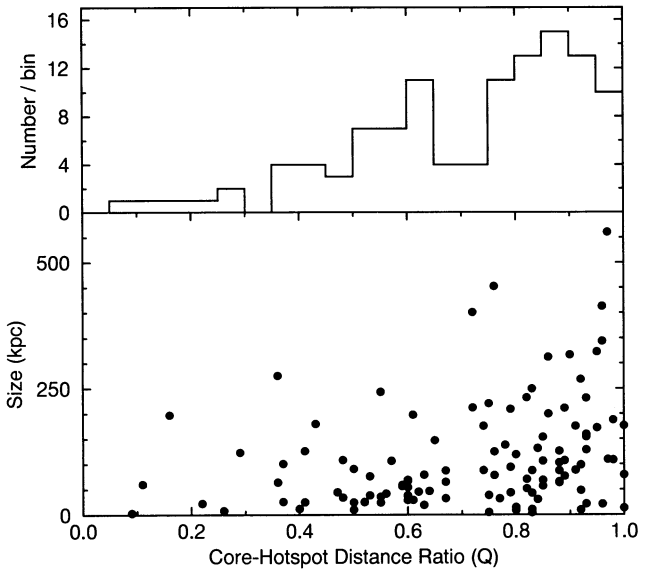

FIG. 3.—Largest apparent size vs. Q (core–hot spot distance ratio) for the quasar sample. As in Fig. 2, the lower panel also shows an upper envelope consistent with projection effects.

smaller sample of 28 radio quasars and concluded that the distributions of sizes and bend angles were consistent with a randomly oriented sample of double-lobed quasars.

There is also an apparent upper envelope in the plot of size versus Q, shown in Figure 3. Fokker (1986) investigated the relation between these two parameters for a large sample of quasars and radio galaxies and suggested that the asymmetry of radio sources was intrinsic and not due to foreshortening or beaming effects. Evidence has been put forward in favor of alternating jet ejection in quasars (HPG; Rudnick & Edgar 1984), which implies an intrinsic source asymmetry, and can explain the lack of sources in the top left corner in Figure 3. We discuss below how this is also a diagnostic of projection effects of bent sources. In our quasar papers we have used the models of Ensman & Ulvestad (1984) to fit the Q distributions. These do allow for time travel and relativistic effects but do not consider bending of the sources, which clearly is present.

4. RADIO SOURCE MODELS

To predict our measured distributions we need to adopt values for the intrinsic properties of EGRSs. Because of the effects of projection, there are very few direct observational constraints on their intrinsic sizes, bend angles, and Q-values. Thus, we look for the simplest choice of reasonable model parameters that can reproduce the observational data, and explore ranges of values, and the sensitivities of the results to them. Our model is the one sketched in Figure 1, oriented with respect to the line of sight. The orientation (Φ) is defined by the angle between the L_2 axis and the line of sight. We calculate the distributions as in Figures 2 and 3 for the models with various values or ranges of Q, bend (α), size (L_1 and L_2), and Φ.

4.1. *Sizes*

The choice of intrinsic size distribution for the model was nontrivial as very little is known about the overall shape of the quasar size distribution. Recent work by Fanti et al. (1990) has suggested that compact steep-spectrum quasars are intrinsically small and are not objects oriented very close to the line of sight as previously thought. When comparing the inferred sizes of the smallest of these objects ($\lesssim$0.2 kpc) to the largest quasars known—2043+745 (770 kpc) and 0729+818 (764 kpc)—it is apparent that quasars do indeed span a wide range of intrinsic sizes.

Figure 4 shows the apparent size distribution for our quasar sample. The distribution can be fitted with a simple exponentially decaying function toward larger apparent sizes. It is important, however, to recognize the possible selection effects that may be present in this distribution.

First, the number of sources in the 0–20 kpc bin is reduced due to the resolutional limits of our radio maps (approximately 4–10 kpc at $z = 2$).

Second, evidence has been put forward for an anticorrelation between lobe size and total radio power (HPG), implying that flux-limited surveys would be biased against large, weak radio sources. However, we have made a strong attempt in our large quasar survey to fill the L-z plane as evenly as possible so as to avoid this effect.

It is important to note that the distribution in Figure 4 is an apparent size distribution, and therefore suffers from foreshortening effects. This increases the numbers of objects in the small size bins while decreasing those in the larger bins. However, for a randomly oriented sample, most sources will lie near the plane of the sky, as the probability of finding a source at an angle Φ to the line of sight goes as $[1 - \cos(\Phi)]$. If this is the case, foreshortening will not have a large impact on the overall shape of the apparent size distribution. If quasars are a highly beamed population, the above assumptions will be incorrect and the distribution will need a scale factor in the size dimension, to a first approximation. For a population seen within a 45° cone, this factor will be less than a factor 2.

For a start, we adopt an intrinsic source size distribution for triple sources as given by Figure 4 (with the exception of the first bin). Physically, we have found this distribution to be consistent with a simple model in which triple sources have random ages, lobe velocities, and lobe growth damping factors due to the intergalactic medium. However, there are no real observational constraints on any of these parameters so they cannot be used in the model. Thus, a decaying exponential was fitted to the data in Figure 4, omitting the first bin due to the observational bias discussed above. After calculating the apparent sizes of the randomly oriented canonical quasars, we

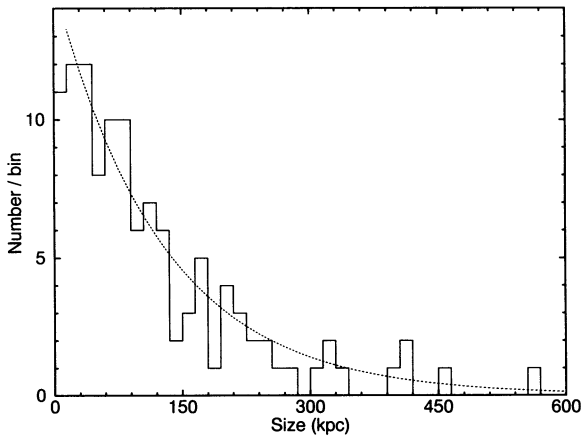

FIG. 4.—Apparent size distribution of quasar sample. The dotted line shows an exponential profile of the form $y \propto e^{-0.0079x}$.

omitted those smaller than 8 kpc to mimic the bias in the observational data. We found that the results are not significantly dependent on the exact shape of this distribution. However, distributions differing strongly from an exponential profile, such as a uniform size distribution, provided poor fits to the data.

4.2. *Core–Hot Spot Distances*

There has been considerable discussion about the observed lobe-length asymmetries in radio quasars. In HPG and NH we discussed the case for alternating ejection, a process in which only one of the jets is active at a time. This model not only accounts for the unequal core–hot spot lengths of many double-lobed EGRSs, but also provides an explanation for objects with one-sided jet structures. We showed that the distribution of Q, the core–hot spot lengths and their differences can be fitted with such a model, where bending effects are neglected.

There are other possible explanations that need to be examined. Many good arguments have been made for the existence of relativistic beaming effects in radio jets. Light-travel time effects due to the relativistic velocities in the jets and lobes can cause an apparent core–hot spot length asymmetry if a source is oriented close to the line of sight. Furthermore, the radiation from the far jet would be beamed away from the observer, rendering it invisible, and giving the appearance of a one-sided jet structure. However, in our double-lobed sources we do not find that the longer side is the brighter, as this would require, so that this is additional support for the alternating model with nonrelativisitc bulk velocities.

In the models we discuss here, we assume zero lobe velocities, so that light-travel time effects are neglected. We examine only the projection effects of stationary bent models.

In choosing the intrinsic core–hot spot distance ratios for the canonical quasars we have adopted two basic forms for the Q-distribution, the first being to assume $Q = 1$ for all sources. The second distribution assumes a random core–hot spot length difference between 0 and 45 kpc. These latter values come directly from the lobe length measures discussed in HPG and NHG.

4.3. *Bend Angles*

Various explanations have been put forward for the noncollinear or "bent" appearance of many quasars. Detailed VLA maps of so-called "wide-angle tail" (WAT) sources show that their exaggerated bends are most likely due to motion of the core through a dense intergalactic medium, which causes the lobes to be swept backward in a direction opposite to the core motion. This effect does not appear to be sufficient, however, to explain the sources with only slight bend angles. These objects instead may have precessing cores that change the direction of the jets (Gower et al. 1982), or may suffer inelastic collisions with a nearby obstruction (Stocke, Burns, & Christiansen 1985). Bends may also be the result of Kelvin-Helmholtz instabilities in the jets (Norman & Hardee 1988; Clarke 1993).

In light of the uncertainties regarding these effects, we have essentially left the bend angle a free parameter in the model and have investigated a variety of possible distributions. In the models we ran, we assumed constant values for the bend and also randomly distributed values within a range. The bend values used are in the range 0° to ~40°. The constant bend models did not provide better fits and are quite unlikely, so we did not pursue them.

5. TESTING THE MODEL FITS

To test how well the models fit the observational size-bend and size-Q distributions, we employ a version of the K-S test modified for use with two-dimensional distributions by Peacock (1983).

The test, described in detail by Fasano & Franceschini (1987), involves dividing the size/bend-angle plane into four quadrants at the position of the first observational data point. The number of observational data points in the first quadrant is calculated, and divided by the total number of observational data points to give a cumulative probability value. This step is also done in the same quadrant for the model points, and the absolute value of the difference of these two probabilities is recorded. The process is then repeated for the other three quadrants. The plane is then divided into four quadrants at the position of the next observational data point, and new differences are found. The largest difference found by this method is known as the D statistic and is a measure of how well the two data sets are correlated. For completely uncorrelated data sets lying in different regions of the plane, the D statistic will be very close to one, so a *low* value of D implies a better fit to the data. When comparing random distributions to the observational data sets, consistent values of $D \simeq 0.66$ were obtained. To be considered a good fit therefore, a particular model should have a D value significantly *lower* than this value.

We discuss several types of model and how well they fit. We discuss mostly the quasar sample, as the data are more reliable and extensive. We then look for consistency in the unified approach between radio galaxies and quasars, using the most successful quasar model.

Tables 2 and 3 show the D values for several model fits, and Figures 5, 6, and 7 show the comparison between models and the data. In the comparisons, we have computed the same

TABLE 2

D STATISTICS FOR EQUAL LOBE ($Q_{\rm intrinsic} = 1$) MODELS

BEND RANGE	$\Phi = 90°$			$\Phi = 60°$			$\Phi = 50°$			$\Phi = 40°$			$\Phi = 30°$			$\Phi = 20°$		
	D_b	D_q	$D_{\rm tot}$	D_b	D_q	$D_{\rm tot}$	D_b	D_q	$D_{\rm tot}$	D_b	D_q	$D_{\rm tot}$	D_b	D_q	$D_{\rm tot}$	D_b	D_q	$D_{\rm tot}$
0°–5°	0.71	0.80	1.51	0.60	0.71	1.31	0.54	0.68	1.22	0.48	0.63	1.11	0.42	0.55	0.97	0.31	0.43	0.73
0°–10°.....	0.50	0.70	1.21	0.39	0.56	0.96	0.35	0.51	0.86	0.29	0.42	0.70	0.23	0.36	0.59	0.16	0.28	0.44
0°–15°.....	0.39	0.63	1.02	0.27	0.45	0.72	0.25	0.39	0.64	0.19	0.31	0.51	0.17	0.27	0.45	0.23	0.19	0.42
0°–20°.....	0.31	0.57	0.88	0.19	0.36	0.55	0.19	0.33	0.51	0.16	0.25	0.41	0.24	0.22	0.46	0.31	0.19	0.50
0°–25°.....	0.25	0.52	0.77	0.15	0.32	0.47	0.19	0.30	0.48	0.20	0.21	0.41	0.29	0.21	0.50	0.38	0.22	0.60
0°–30°.....	0.21	0.46	0.67	0.15	0.28	0.42	0.22	0.26	0.48	0.25	0.17	0.42	0.34	0.20	0.53	0.42	0.25	0.67
0°–35°.....	0.19	0.42	0.60	0.17	0.26	0.42	0.25	0.23	0.48	0.29	0.14	0.43	0.38	0.20	0.57	0.44	0.29	0.73
0°–40°.....	0.16	0.37	0.53	0.20	0.23	0.43	0.28	0.22	0.50	0.33	0.15	0.48	0.41	0.22	0.63	0.46	0.32	0.78

NOTES.—D_b: Goodness of fit (D) statistic for size-bend distributions (see § 5); D_q: Goodness of fit (D) statistic for size-Q distributions (see § 5).

TABLE 3

D STATISTICS FOR UNEQUAL LOBE ($Q_{intrinsic} \neq 1$) MODELS

BEND RANGE	$\Phi = 90°$			$\Phi = 60°$			$\Phi = 50°$			$\Phi = 40°$			$\Phi = 30°$			$\Phi = 20°$		
	D_b	D_q	D_{tot}	D_b	D_q	D_{tot}	D_b	D_q	D_{tot}	D_b	D_q	D_{tot}	D_b	D_q	D_{tot}	D_b	D_q	D_{tot}
0°–5°	0.67	0.14	0.81	0.59	0.15	0.74	0.55	0.13	0.69	0.47	0.15	0.62	0.38	0.15	0.53	0.29	0.17	0.46
0°–10°.....	0.48	0.14	0.62	0.37	0.16	0.53	0.37	0.15	0.52	0.27	0.16	0.43	0.20	0.16	0.35	0.17	0.20	0.37
0°–15°.....	0.37	0.14	0.52	0.26	0.15	0.41	0.25	0.16	0.41	0.17	0.17	0.34	0.16	0.16	0.32	0.26	0.22	0.49
0°–20°.....	0.30	0.14	0.45	0.18	0.17	0.35	0.17	0.17	0.34	0.15	0.19	0.34	0.24	0.19	0.43	0.33	0.26	0.59
0°–25°.....	0.26	0.15	0.41	0.16	0.18	0.34	0.15	0.19	0.34	0.23	0.19	0.43	0.29	0.21	0.50	0.38	0.27	0.65
0°–30°.....	0.20	0.15	0.35	0.17	0.20	0.36	0.19	0.21	0.41	0.27	0.21	0.49	0.34	0.25	0.59	0.40	0.30	0.70
0°–35°.....	0.17	0.16	0.32	0.19	0.20	0.40	0.25	0.23	0.48	0.31	0.23	0.54	0.37	0.27	0.64	0.43	0.33	0.76
0°–40°.....	0.14	0.16	0.30	0.22	0.21	0.43	0.29	0.24	0.53	0.34	0.24	0.58	0.39	0.28	0.67	0.46	0.36	0.82

NOTES.—D_b: Goodness of fit (D) statistic for size-bend distributions (see § 5); D_q: Goodness of fit (D) statistic for size-Q distributions (see § 5).

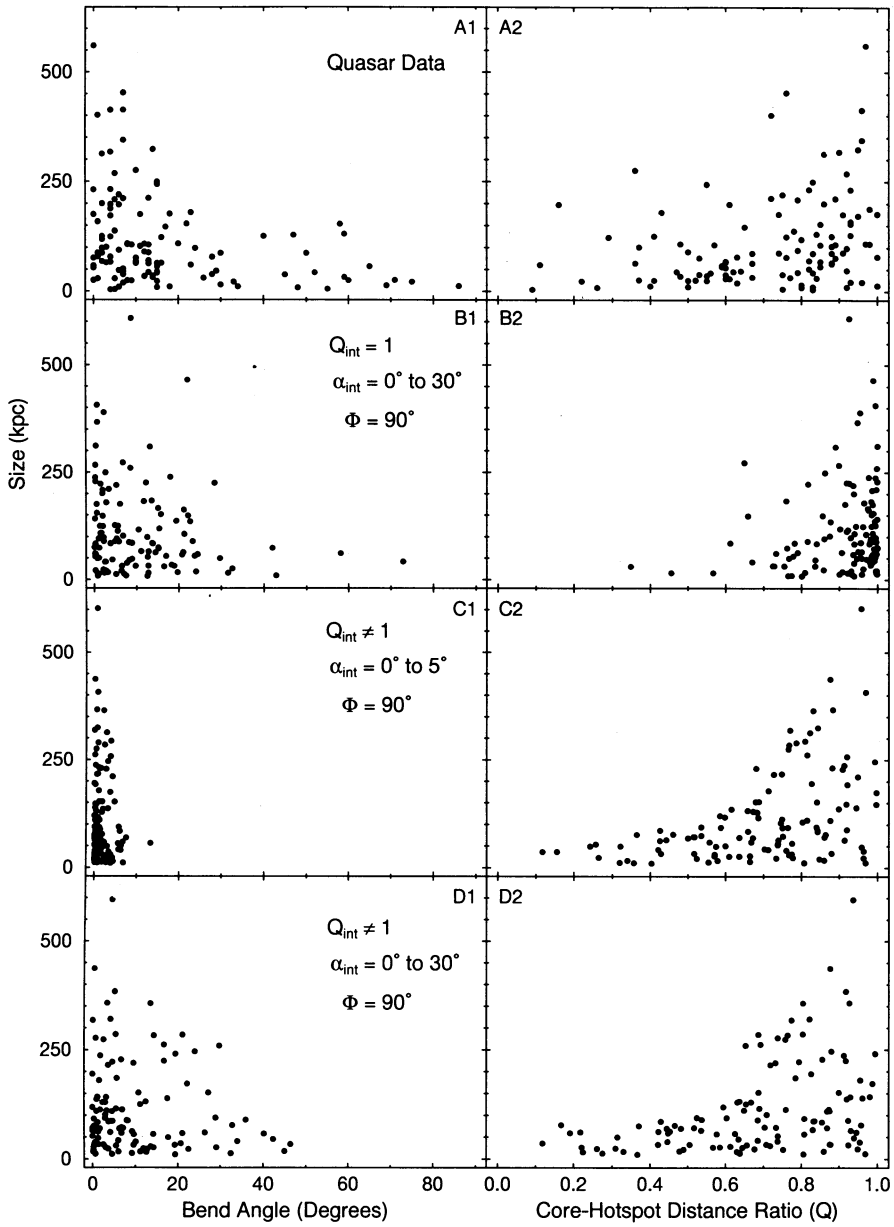

FIG. 5.—Radio quasar size vs. bend and size vs. Q distributions. Panels A1 and A2 contain the quasar data presented in Figs. 2 and 3, while panels B, C, and D show distributions for a set of randomly oriented canonical quasars (see § 5). The parameters used in each model are indicated as follows: models with $Q_{int} = 1$ have equal core–hot spot distances (i.e., $L_1 = L_2$), and the intrinsic bend angle range is given by α_{int}. Panel B2 shows that models with equal core–hot spot distances do not provide a good fit to the observed Q distribution. It is also apparent from panel C1 that a large range of intrinsic bend angles is required to reproduce the observed bend angle distribution.

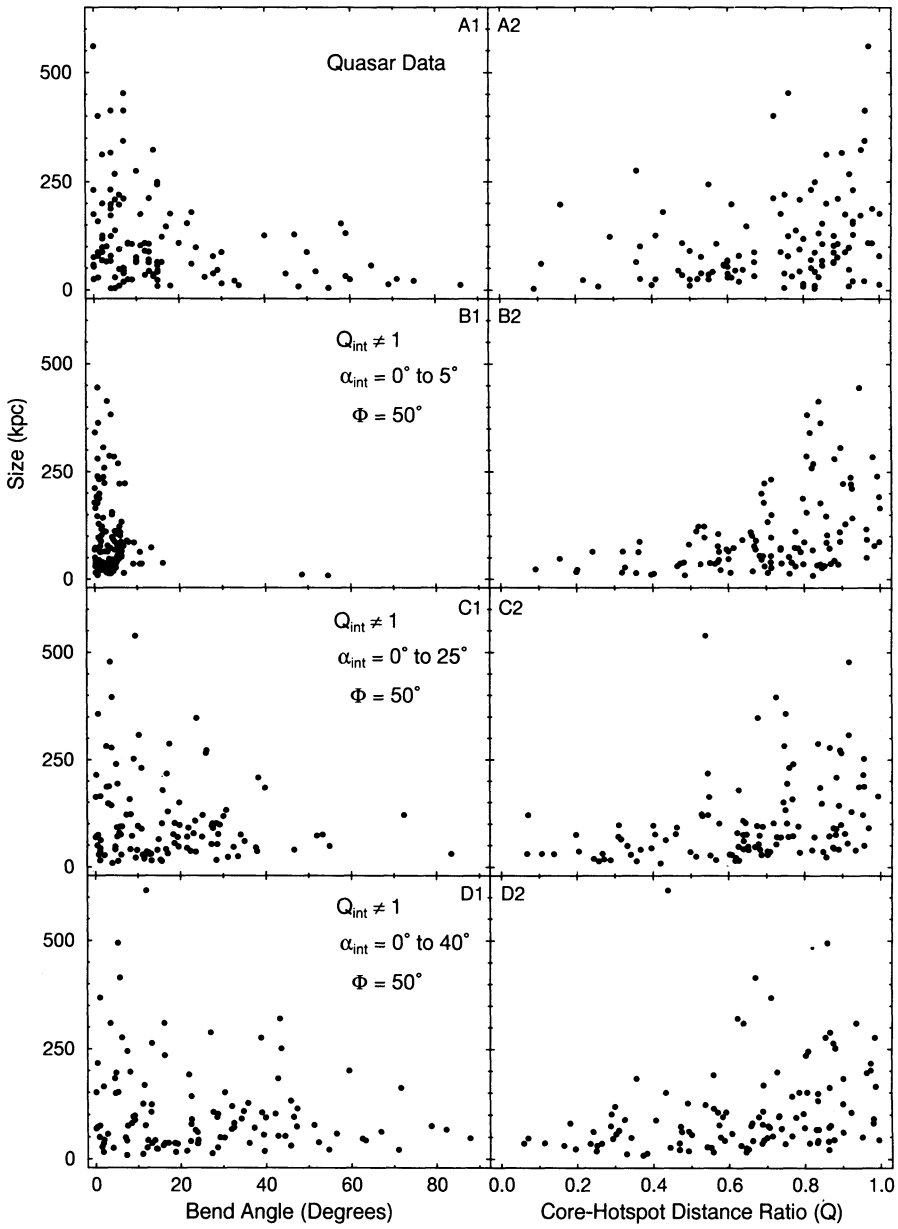

FIG. 6.—Radio quasar size vs. bend and size vs. Q distributions for orientation biased models. Again the quasar data are presented in panels A1 and A2 for comparison to the model distributions in panels B, C, and D. These latter panels show the predicted distributions for a set of canonical quasars randomly oriented within a viewing cone of half-angle $\Phi = 50°$ (see Fig. 8). Such a scenario is predicted by the unified model for radio galaxies and quasars (see § 5). Again it is apparent from panel B1 that a large range of intrinsic bend angle in the model is required to reproduce the data. The model shown in panel C($Q_{int} \neq 1$, $\alpha_{int} = 0°$–$25°$, and $\Phi = 50°$) provides the best fit to the data.

number of model points as data points for the quasars. In the smaller radio galaxy sample we have also computed models with 500 points, to reduce "noise" in the comparison.

In Figure 5 we show the size-bend and size-Q plots for several equal- and unequal-lobe ($Q_{\text{intrinsic}} = , \neq 1$) models using different bend angle ranges. The quasar data are presented in panels A1 and A2. The observed size-Q distribution in panel A2 is much better fitted by the unequal-lobe ($Q_{\text{intrinsic}} \neq 1$) models (C2 and D2). These models have significantly lower D_q values in Tables 2 and 3.

Examining the bend angle distributions on the left side of Figure 5 and the D_b statistics in Tables 2 and 3, it is apparent that the models with the largest range of intrinsic bend angle provide the best fits to the data. However, these models still cannot account for the large quantity of observed triple sources with apparent bends $\gtrsim 40°$.

The quality of the fits improves significantly when models in which quasars are viewed only within some cone of half-angle Φ around the source axis (see Fig. 8) are used. The effect of introducing this "orientation bias" is to increase the probability of seeing a source aligned close to the line of sight. Thus, these models yield a greater number of sources with large apparent bends, which is in accordance with the observed data. Three such models are shown in Figure 6. As was the case with the unbiased ($\Phi = 90°$) models, the unequal-lobe models provide the best fits to the size-Q data. Unlike the unbiased

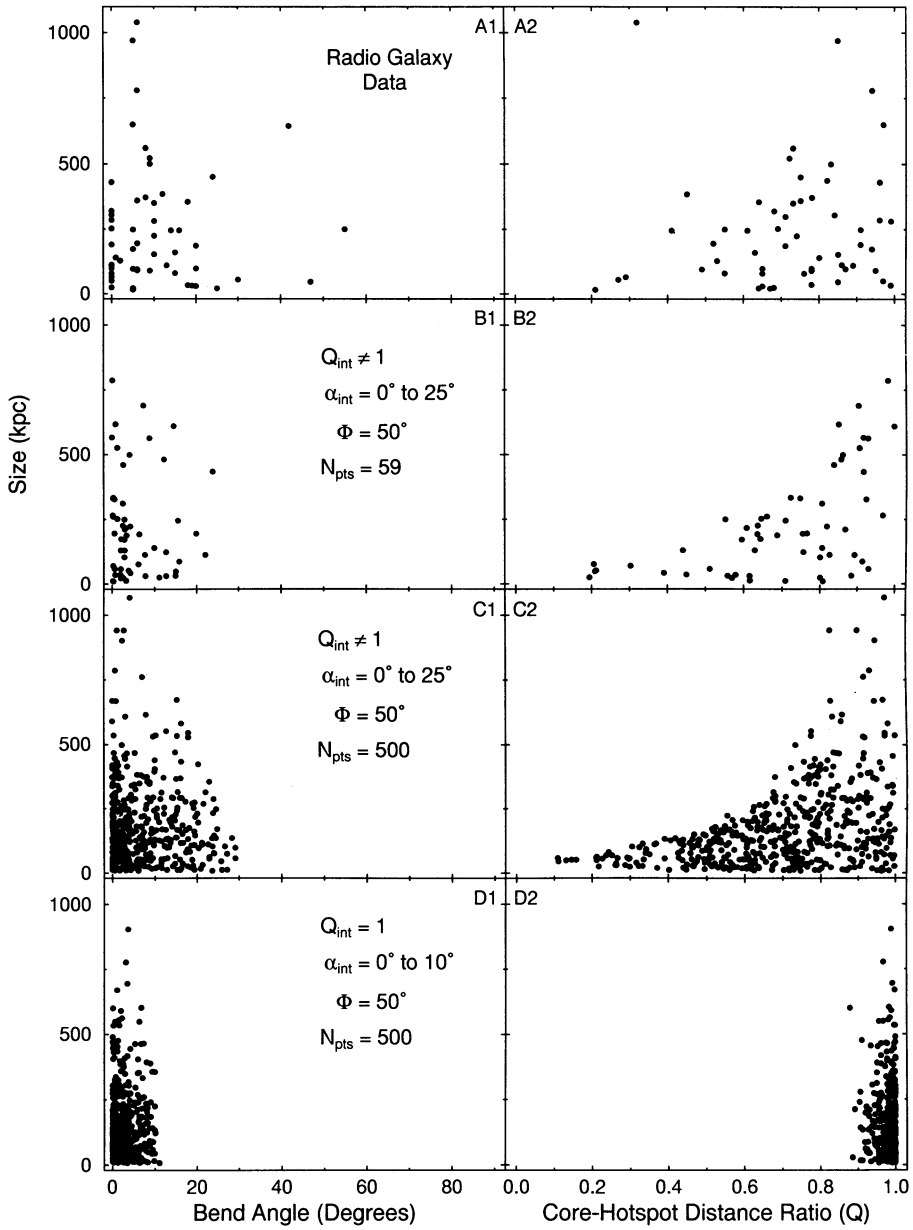

FIG. 7.—Radio galaxy size vs. bend and size vs. Q distributions. The radio galaxy data of Hutchings et al. (1994) are shown in panels A1 and A2. Panels B, C, and D show the distributions for randomly oriented canonical quasars that lie *outside* a viewing angle cone of $\Phi = 50°$. According to the unified model, these objects would be classified as radio galaxies. Panel B shows the resulting distribution using the best quasar fitting parameters ($Q_{int} \neq 1$, $\alpha_{int} = 0°$–$25°$) and displays a strong similarity to the radio galaxy data. Panel C shows this same distribution, but with 500 points plotted. In panel D we see that a model using a small range of intrinsic bend angle and an equal core–hot spot distance ratio does not provide a good fit to the radio galaxy data.

models however, the best-fitting viewing-cone models have intermediate ranges of intrinsic bend angle (e.g., 0°–20°, 0°–25°). This finding, along with the overall lower D values of the viewing-cone models in Tables 2 and 3, allows us to conclude that the observed morphological characteristics of the radio quasars in our sample are consistent with those of an unequal lobed, moderately bent population of radio sources, randomly oriented within a viewing cone of half-angle Φ. Based on our K-S tests, the overall best fit model has $Q_{int} \neq 1$, an intrinsic bend angle range of 0°–25°, and a viewing cone of $\Phi = 50°$.

In the unified scheme of Barthel (1989), radio galaxies are the same sources as the radio quasars in our model, viewed outside a cone of half-angle Φ (Fig. 8). Thus it is of considerable interest to test this hypothesis. The radio galaxy samples discussed by Hutchings et al. (1994) were selected, observed, and measured in the same way as the quasars we have discussed and are suitable for comparison. Figure 7 shows these data, and the fits using the parameters of the best quasar model. Except for three very bent sources, the fit is good here too, providing support for such a model. We note that the size distribution of the Hutchings et al. (1994) galaxies has a larger upper envelope, and the bend angles are smaller, as expected for this scenario.

We may summarize the model fitting by the following. There is an intrinsic asymmetry in the EGRS lobe lengths, which is consistent with the alternating ejection hypothesis. The lack of beaming within the lobes and the existence of one-sided

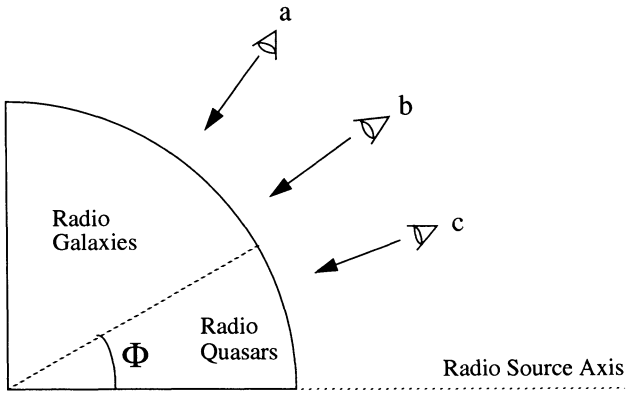

FIG. 8.—Unified model for radio galaxies and quasars, showing viewing cone angle Φ definition. A radio source with its core and lobes aligned along the axis as shown would be classified as a radio galaxy by observers *a* and *b*, while observer *c* would classify it as a quasar.

sources is also evidence for nonrelativistic alternating ejection. The size difference assumed in our model is consistent with the alternating ejection model fit to the Q distribution of HPG, and our model is an elaboration of this. The best fit requires the quasar population to be viewed within a cone of angle 50°, which is consistent with the radiation cone angles seen in nearby active galactic nuclei, such as NGC 1068 (Evans et al. 1991), and the hidden Seyfert 1 model for Seyfert 2 galaxies. We also find consistency with the radio galaxy morphology for the same parameter model.

6. UNIFICATION MODELS FOR AGN

While we have shown a good fit to a complex data set that supports a unified model for EGRSs, it is important to assess the strength of this conclusion. First, much depends on the lack of relativistic bulk velocity effects in the lobes and hot spots. If expansion velocities are even mildly relativistic (0.3c, say) then light travel times will introduce further asymmetries of size and flux. We cannot rule this out from the flux/size tests, especially as intrinsic asymmetries must play a role in that test too. We also note that radio galaxies have a lack of one-sided sources, which suggests that they either are a different population or that the radiation really is beamed enough to make this effect important in quasars seen end-on.

The existence of bright core radio galaxies and a few very bent radio galaxies also poses a problem. These may represent examples of partially beamed or collimated core radiation, or sources that have greatly changed direction during their lifetime. There has also been increasing evidence that superluminal motion may be ubiquitous among the various classes of AGNs. This is troubling for some unified schemes, since superluminal motion requires a core jet aligned close to the line of sight. To date the cores of radio galaxies have been generally too faint for detailed VLBI observations, so it has not been confirmed whether they too display this phenomenon.

We also note the problem with host galaxy colors of quasars and radio galaxies being different, and the interaction status of radio galaxies and quasars being different (Hutchings 1987). Both of these complicate Barthel's (1989) simple unified scheme and the distributed morphology model. They indicate that there may be differences other than orientation which distinguish radio galaxies and quasars. Finally, the number counts of radio galaxies and quasars also suggest that orientation may be the dominant parameter only in some quantities; thus the results of our orientation modeling lend support to, but must not be considered proof of Barthel's (1989) unified scheme.

7. CONCLUSIONS

In this paper we have shown the observed morphological characteristics of a sample of 114 radio quasars to be well represented by a population of unequal-lobed, intrinsically bent ($\alpha_{\rm int} = 0°$–$25°$) radio sources, randomly oriented within a viewing cone of angle $\Phi = 50°$. The parameter values quoted represent the best overall fit to the data examined and should be regarded as typical rather than definitive values that apply to all sources.

The predicted characteristics of sources lying *outside* this viewing cone were found to be consistent with those of a sample of 59 radio galaxies observed by Hutchings et al. (1994). These findings are in accordance with the unified model of Barthel (1989), which postulates that radio galaxies are objects oriented close to the plane of the sky, while radio quasars are objects seen nearly end-on. These conclusions are strong evidence that orientation is a major parameter in differentiating radio galaxies and quasars, but we caution against this as "proof" that there are no intrinsic differences as well. This work should be extended to larger, unbiased samples when they are available.

M. L. L. wishes to acknowledge a research grant from David Hartwick, Chris Pritchet, and Don VandenBerg of the University of Victoria.

REFERENCES

Barthel, P. D. 1989, ApJ, 336, 606
Barthel, P. D., & Miley, G. K. 1988, Nature, 333, 319
Chyzy, K. T., & Zieba, S. 1993, A&A, 267, L27
Clarke, D. A. 1993, private communication
Ensman, L. M., & Ulvestad, J. S. 1984, AJ, 89, 1275
Evans, I. N., Ford, H. C., Kinney, A. L., Antonucci, R. R. J., Armus, L., & Caganoff, S. 1991, ApJ, 369, L27
Fanti, R., Fanti, C., Schilizzi, R. T., Spencer, R. E., Rendong, Nan, Parma, P., van Breugel, W. J. M., & Venturi, T. 1990, A&A, 231, 333
Fasano, G., & Franceschini, A. 1987, MNRAS, 225, 155
Fokker, A. D. 1986, A&A, 156, 315
Gopal-Krishna, & Kulkarni V. K. 1992, A&A, 257, 11
Gower, A. C., Gregory, P. C., Hutchings, J. B., & Unruh, W. G. 1982, ApJ, 262, 478
Gower, A. C., & Hutchings, J. B. 1984, ApJ, 89, 1658 (GH)
Hewitt, A., & Burbidge, G. 1989, ApJS, 63, 1
Hough, D. H., & Readhead, A. C. S. 1989, AJ, 98, 1208
Hutchings, J. B. 1987, ApJ, 320, 122
Hutchings, J. B., Price, R., & Gower, A. C. 1988, ApJ, 329, 122 (HPG)
Hutchings, J. B., Neff, S. G., Weadock, J., Roberts, L., Ryneveld, S., & Gower, A. C. 1994, AJ, 107, 471
Kaphai, V. K. 1990, in Parsec Scale Radio Jets, ed. J. A. Zensus & T. J. Pearson (Cambridge: Cambridge Univ. Press), 304
Kapahi, V. K., & Saikia, D. J. 1982, J. Astron. Astrophys., 3, 465
Lister, M. L., Gower, A. C., & Hutchings, J. B. 1994, in preparation (LGH)
Neff, S. G., & Hutchings, J. B. 1990, AJ, 100, 1441 (NH)
Neff, S. G., Hutchings, J. B., & Gower, A. C. 1989, AJ, 97, 1291 (NHG)
Norman, M. L., & Hardee, P. E. 1988, ApJ, 334, 80
Padovani, P., & Urry, C. M. 1992, ApJ, 387, 449
Peacock, J. 1983, MNRAS, 202, 615
Rudnick, L., & Edgar, B. K. 1984, ApJ, 279, 74
Scheuer, P. A. 1987, in Superluminal Radio Sources, ed. J. A. Zensus & T. J. Pearson (Cambridge: Cambridge Univ. Press), 104
Stocke, J. T., Burns, J. O., & Christiansen, W. A. 1985, ApJ, 299, 799
Teerikorpi, P. 1984, A&A, 132, 179